Journal of Fluids Engineering

The following publication Wen, X., & Tang, H. (2017). Dye visualization of in-line twin synthetic jets in crossflows—a parametric study. Journal of Fluids Engineering, 139(9), 091203 is available at https://doi.org/10.1115/1.4036410.

# Dye visualization of in-line twin synthetic jets in crossflows - a parametric study

**Xin Wen**[1]
School of Mechanical Engineering
Shanghai Jiao Tong University, Shanghai, 200240, China
wenxin84@sjtu.edu.cn

**Hui Tang**
Department of Mechanical Engineering
The Hong Kong Polytechnic University, Kowloon, Hong Kong SAR, China
h.tang@polyu.edu.hk

## ABSTRACT

*This paper presents a parametric study on the interaction of twin circular synthetic jets (SJs) that are in line with a crossflow over a flat plate. The resulting vortex structures under different actuation and flow conditions are investigated using two-plane color dye visualization in a water tunnel. The influence of four independent non-dimensional parameters, i.e., the Reynolds number $Re_L$, Strouhal number St, velocity ratio VR, and phase difference $\Delta\phi$, on the behavior of the twin SJs is studied. It is found that the increase of Reynolds number causes the SJ-induced vortex structures more turbulent, making the twin SJ interaction less organized. The increase of velocity ratio pushes the occurrence of interaction further away from the wall, and makes the resulting vortex structures more sustainable. The Strouhal number has no obvious influence on the interaction. And three types of vortex structures are observed under different phase differences: one combined vortex, two completely separated vortices, and partially interacting vortex structures. Based on this parametric study, a simple model is proposed to predict the resulting vortex pattern for the twin SJ interaction.*

[1] Corresponding author.

## 1. INTRODUCTION

Synthetic jet (SJ) is a promising means for active flow control due to its ability of injecting non-zero net momentum into ambient flows with zero net mass flux. A typical SJ actuator consists of a cavity with an oscillatory diaphragm on one side and an orifice on the other. The out-of-plane oscillation of the diaphragm generates a succession of vortex structures that propagate away from the orifice, forming a “synthetic jet”. Since proposed, the SJ technology has been applied in many applications as an active flow means, including flow separation control [1-6], mixing control [7-9], and turbulence control [10].

The vortex structures induced from the interaction of SJs with crossflows play a very important role in flow control. For example, a circular SJ issued in a crossflow produces a group of streamwise vortices that are capable of enhancing momentum exchange between the boundary layer and outer flow [11-13]. Depending on the jet-to-freestream velocity ratio and dimensionless stroke length, three types of vortex structures can be observed, i.e., hairpin vortices, stretched vortex rings, and tilted vortex rings [14-16]. Further investigations revealed that hairpin vortices and stretched vortex rings are responsible for flow separation delay [17,18].

In real world applications, it is SJ arrays that are usually implemented instead of single SJs. Using two slot SJ actuators, Hasnain et al. [19] found that the point of flow separation on a two-dimensional (2D) cylinder can be delayed by 20% at specific phase difference between the two actuators. Zhao et al. [20] confirmed that two slot SJ actuators generally have better performances than single SJ in delaying flow separation

on a 2D airfoil. In addition, the preferable phase difference between the two actuators varies under different angles of attack. For the circular SJs, due to the complex 3D flow structures, the interaction between neighboring SJs in crossflows leads to more complex flow structures, which may enhance or reduce the flow control effectiveness. To determine the interaction effect, a profound understanding of these vortex structures is desired. However, compared to those on single-SJ induced vortex structures, investigations on SJ-array induced vortex structures in crossflows are very limited. Extensive studies on a similar case, i.e. multiple continuous jets in crossflows, can still shed some light on this new flow phenomenon. Kolar et al. [21] performed hot-wire measurements on twin jets in crossflow and found that, with in- line arrangement, the counter-rotating vortex pairs from the two jets merge into a single and stronger counter-rotating vortex pair. Similar constructive interaction is also found between twin circular SJs in crossflow under the same jet configuration [22]. The authors' previous works [23-25] found that the resulting flow structures change significantly with the change of phase difference between twin SJs, and found that twin SJs is much more effective in flow separation control than single SJs. Liddle & Wood [26] visualized the flow structure under different configuration yaw angles (the angle between the crossflow direction and the line connecting the orifice centers of the two actuators) and phase differences using oil-flow and hotwire anemometry techniques. Although very interesting results were obtained, they did not get a holistic picture of the resulting vortex structures. Iai et al. [27] and Honami & Motosuke [28] did a series of PIV measurements on two circular SJ actuators arranged in line with a channel flow,

investigating the effects of velocity ratio and phase difference between the two SJs on the resulting vortex structures. Their vortex structures visualized using vorticity iso-surfaces and velocity vector fields are not well represented due to low quality images. In addition, in their results it is hard to differentiate the contribution of individual SJs to the resulting vortex structures due to the same color used for the iso-surfaces, making the in-depth analysis difficult.

As a continuous effort towards a comprehensive understanding of the interaction of SJ arrays in crossflows, the present study following the authors' previous works [23, 24] aims to conduct a parametric study on the interaction of in-line, twin circular SJs in laminar crossflows over a flat plate. The behavior of the interacting vortex structures will be investigated under different flow and actuation conditions and compared with the corresponding vortex structures produced by single SJs.

## 2. Methodology

### 2.1 Dimensional analysis

For a given SJ actuator perpendicularly issuing circular SJs into a zero-pressure-gradient flat-plate crossflow, the behavior of the SJ depends on the following five physical parameters: the actuator orifice diameter $D_o$ and operating frequency $f$ , time-averaged jet velocity $\bar{U}_o$, crossflow velocity $U_\infty$, and fluid viscosity $v$. Behavior of the SJ is associated with five non- dimensional parameters, i.e., the non-dimensional stroke length $L$, the stroke length based Reynolds number $Re_L$, the Stokes number $S$, the Strouhal number $St$, and the jet-to-crossflow velocity ratio $VR$. The first three are only associated with the SJ and independent of the crossflow, whereas the last two are

associated with both. The non-dimensional stoke length *L* describing the relative length of fluid column ejected during the blowing stroke is defined as

$$L = \frac{L_o}{D_o} = \frac{\overline{U}_o}{fD_o} \tag{1}$$

where $L_o$ is the stroke length representing the actual length of the fluid column, and $\overline{U}_o$ is the time-averaged blowing velocity over an entire actuation cycle. The stroke length based Reynolds number, $Re_L$, represents the ratio of inertial forces to viscous forces

$$Re_L = \frac{\overline{U}_o L_o}{\nu} \tag{2}$$

It characterizes SJ vortex circulation and hence is a useful indicator of vortex strength [29, 30]. The Stokes number *S* is defined as the ratio of unsteady forces to viscous forces

$$S = \sqrt{\frac{2\pi f D_o^2}{\nu}} \tag{3}$$

Zhou et al. [31] revealed that a minimum Stokes number is required to roll up SJ vortices.

When a crossflow is introduced, the Strouhal number *St* is defined

$$St = \frac{fD_o}{U_\infty} \tag{4}$$

*St* is used to describe the frequency of the SJ in the crossflow, determining the spacing of successive SJ vortex structures in the crossflow direction: the larger the *St* value, the smaller the spacing. The velocity ratio *VR* quantifies the ratio of the SJ velocity to the crossflow velocity

$$VR = \frac{\overline{U}_o}{U_\infty} \tag{5}$$

All the above parameters are used to characterize the behavior of single SJs in crossflows. If two identical SJ actuators are placed in line with the crossflow and operated with the same SJ velocities and frequencies, two additional non-dimensional

parameters are required to describe the resulting flow. One is $d/D_o$, the non-dimensional center-to-center distance between the two actuator orifices, and the other one is $\Delta\phi$, the operational phase difference of the two actuators.

From the above analysis, there are in total seven non-dimensional parameters that can be used to characterize the behavior of in-line twin SJs in crossflows. Note among the first five parameters, only three are independent. That is, if $Re_L$, $St$ and $VR$ are chosen as the independent parameters, $L$ and $S$ can be expressed as

$$L = \frac{VR}{St}, \qquad S = \sqrt{2\pi \frac{Re_L}{L^2}} = \sqrt{2\pi Re_L \left(\frac{St}{VR}\right)^2} \tag{6}$$

To make the present investigation more focused, the non-dimensional distance between the twin SJAs is fixed at $d/D_o = 2$. Hence the behavior of the in-line twin SJs in crossflows can be characterized by four independent non-dimensional parameters, i.e., $Re_L$, $St$, $VR$, and $\Delta\phi$.

**2.2 Test rig**

A series of experiments is conducted in a water tunnel. Its test section is 1 m (L) × 0.45 m (W) × 0.45 m (H), in which a uniform steady flow with a speed up to 0.2 m/s can be generated. The crossflow was produced along a test plate parallel to the water flow. Fig. 1a shows a sketch of the test plate as well as the coordinate system used in the present study. The test plate is 750 mm long and has a 1:5 elliptical leading edge that helps to minimize possible flow separation. As shown in the side view of Fig. 1a, two SJ actuators are mounted on the test plate. Each actuator has a cylindrical cavity

with an orifice plate at its bottom side and a moving diaphragm clamped to its top side, as depicted in the close view in Fig. 1b. The cavity has a diameter of $D_c$ = 82 mm and a height of $H$ = 25 mm, and the orifice has a diameter of $D_o$ = 5 mm and depth of $h$ = 5 mm. In the present study, the orifices of the two actuators are not located at the center of their respective orifice plates. Instead, they are designed to be close to each other, with the center-to-center distance fixed at $d$ = 10 mm, i.e., $d/D_o$ = 2. The centers of these two orifices are aligned with the crossflow direction, and their midpoint is located at 470 mm downstream from the test plate's leading edge. As depicted in Fig. 1a, the origin of the coordinate system used in the present study is set at this midpoint, with the $x$ axis pointing to the crossflow flow direction, $y$ axis downward, and $z$ axis to the spanwise direction.

The diaphragm of the actuators has a diameter of $D_d$ = 45 mm, whose center is attached to a permanent magnetic shaker (LDS V201 from Brüel & Kjær) via a steel rod. When in operation, the diaphragm oscillates in a sinusoidal manner with tunable peak-to-peak displacement $\Delta$ and frequency $f$. If the working fluid is incompressible as in the present study, the time-averaged jet velocity over an entire actuation cycle $T$ can be estimated in terms of $\Delta$ and $f$

$$\bar{U}_o = \frac{1}{T}\int_0^{T/2} u_o(t)dt = \Delta f\left(\frac{D_d}{D_o}\right)^2 \quad (7)$$

where $u_o(t)$ is the instantaneous jet velocity. With $\bar{U}_o$ calculated using equation 7, all the non-dimensional parameters described in section 2.1 can be estimated using equations 1-6.

If both the SJ actuators are in operation, the oscillation amplitude and frequency of their diaphragms are controlled by two synchronized sine wave signals using LabVIEW. The operational phase difference between these two actuators can be tuned with a resolution of 1°. To read the oscillation amplitude, the motion of the diaphragm center is measured using an eddy current displacement sensor (ECL202 from Lion Precision).

**2.3 Visualization system**

To visualize and differentiate the twin SJs in the crossflow, food dye of two different colors was used to fill the SJ actuators. The upstream actuator was filled with red dye and the downstream actuator filled with green dye. The dye was premixed with methanol to achieve a density very close to water's. In the experiments, a high-speed camera (MotionBLITZ EoSens) was used to capture the dye pattern produced by the SJs from the side view, and a DSLR camera (Cannon EOS 60D) was used underneath the water tunnel test section to form the plan view. Both the cameras worked at the same frame rate of 60 fps with a resolution of about 13 pixels per mm or 65 pixels per orifice diameter $D_o$, providing a two-plane dye visualization of the twin SJs as depicted in Fig. 2.

**2.4 Test conditions**

In the present dye visualization study, ten cases were investigated as summarized in Fig. 3. Laminar boundary layers were generated along the test plate with crossflows of three different speeds, i.e., $U_\infty$ = 0.028, 0.055, and 0.110 m/s. The

momentum-thickness based Reynolds numbers at the midpoint of the two orifice centers are $Re_\vartheta$ = 76, 106, and 150, respectively.

Previous studies have revealed that the non-dimensional stroke length $L$ needs to be greater than about 0.5 to ensure SJ formation [32, 33] and less than about 4 to avoid the saturation of primary vortex rings and generation of secondary vortex rings [33, 34]. In this $L$ range, the Stokes number $S$ is suggested to be greater than 8.5 to ensure the rollup of vortex rings [31], which is important for SJ-based flow control. In addition, depending on different combinations of $Re_L$, $St$, and $VR$ values, three types of vortex structures can be induced by single SJs issued into a crossflow, i.e., hairpin vortices, stretched vortex rings, and tilted vortex rings [14]. Both hairpin vortices and stretched vortex rings are capable of delaying flow separation. For these two types of vortex structures, Jabbal & Zhong [14] found an upper limit of $VR \approx 0.4$ ($0.1 < VR < 0.32$ for hairpin vortices; $0.2 < VR < 0.38$ for stretched vortex rings). Therefore, the actuator diaphragm oscillates at selected amplitudes and frequencies such that all the test cases fall in the range of $0.5 < L < 4$, $S > 8.5$, and $VR < 0.4$. Note for each case there are one single SJ case plus four sub-cases with different phase difference, i.e., $\Delta\phi = 0, \pi/2, \pi$, and $3\pi/2$, hence the total number of cases under investigation is 50.

To better describe the twin SJ interaction, single SJs issued from the upstream actuator for the listed ten cases were also visualized as benchmark. Although not presented here, a simple test has confirmed that the influence on the single SJ due to the existence of the non-operating downstream actuator is negligible. Therefore the orifice of the downstream actuator was not covered during the experiments.

## 3. Results and Discussion

### 3.1 Evolution of single and twin SJs in crossflows

A sequence of snapshots showing the evolution of single and twin SJs in case 4 is presented in Fig. 4. Note for better presentations, all the side-view images hereinafter are adjusted such that the crossflow comes from left and the SJs are issued upwards. In addition, the timing for the SJ actuators is defined such that $t = 0$ corresponds to the moment when the upstream actuator reaches its maximum blowing. In Fig. 4, the evolution of the single SJ issued from the upstream actuator is shown in the upper two rows. It is shown that, after emerging at the orifice exit, the vortex ring gradually tilts towards downstream ($t = 0.16T$ ). Its upstream branch is weakened by the resident vorticity in the boundary layer that has the opposite-signed vorticity. As time evolves to $t = 0.46T$ , the upstream branch vanishes, and the downstream branch starts getting stretched by the shear stress in the boundary layer, forming two legs that are retarded at the orifice exit (see the plan view). At $t = 0.72T$, the upstream ends of the two vortex legs move downstream, and the vortex head reaches the edge of the boundary layer (the horizontal line). As time evolves, the vortex head moves faster outside the boundary layer and tends to be upright due to smaller shear out there, while the legs keep stretching, making the entire vortex structure elongate further in the streamwise direction.

When the in-line twin SJs are issued into the crossflow with zero phase difference, the SJ produced by the upstream actuator evolves in the same way as the single SJ does as shown in first three snapshots of the lower two rows, whereas the SJ

produced by the downstream actuator behaves slightly differently. Due to the shielding effect of its upstream counterpart, the vortex structure generated from the downstream actuator appears less tilted. When both vortex structures start stretching at $t$ = 0.46$T$, the mid portion of the downstream vortex legs is entrained into the head of the upstream vortex, resulting in the touching of the two vortex structures. This entrainment is a combined result of clockwise rotation of the upstream vortex head and the upwash flow between the two legs of the upstream vortex that is induced by the counter-rotating of the two legs. As time evolves to $t$ = 0.72$T$, the entire legs of the downstream vortex are lifted up by the upwash flow and entrained between the two legs of the upstream vortex, starting rotating around those legs. As such, the interaction between the twin SJs produces a more complex vortex structure than that produced by a single SJ, as shown at $t$ = 0.94$T$. Furthermore, it is found that the upstream vortex of the twin SJs travels a little bit slower than that of the single SJ, and its penetration into the crossflow is slightly weaker. Obviously this is because of the influence of the downstream vortex.

### 3.2 Influence of $Re_L$, $St$, $VR$, and $\Delta\phi$

The influence of the first three non-dimensional parameters, i.e., $Re_L$, $St$, and $VR$, on vortex structures induced by both single and twin SJs is studied and presented in Figs. 5-7. From previous findings on single SJs [14,30], the Reynolds number $Re_L$ determines the strength of circulation carried by SJ-induced vortices, the Strouhal number $St$ characterizes the streamwise distance between the consecutive vortices, and the jet-to-

freestream velocity ratio *VR* decides the orientation of emerging vortex structures as well as the trajectory of SJs in the crossflow. Figs. 5-7 not only confirm these findings for single SJs, but also reveal the influence of these three parameters on the interaction of the in-line twin SJs. Fig. 5 compares case 4 and case 10, the former having the same *St* and *VR* values but a half of the $Re_L$ value of the latter's. The increase of $Re_L$ results in the increase of circulation carried by each vortex. It also induces instability, making the vortex structures seem more turbulent. As a result, the interaction between the twin SJs is less organized (see case 10 in Fig. 5). Fig. 6 compares case 1 and case 8, the former having the same $Re_L$ and *St* values but twice of the *VR* value of the latter's. The increase of *VR* results in the increase of the orientation angle between the emerging vortex structures and the flat plate. It also pushes the trajectories of the vortex heads further away from the wall. As such, the interaction of the twin SJs occurs in a higher region, and the resulting vortex structures are more sustainable due to the escape of the near-wall high-shear region. Fig. 7 compares case 2 and case 8, the former having the same $Re_L$ and *VR* values but a half of the *St* value of the latter's. It confirms that the increase of *St* results in the decrease of the streamwise spacing between two consecutive vortex structures. But the influence of St on the twin SJ interaction seems not obvious. Note in case 8, since the non-dimensional stroke length $L = 1.2$ does not exceed the SJ formation criterion ($L > 0.5$) too much, the generated SJs appear much weaker than those in case 2 where $L = 2.4$.

The fourth independent non-dimensional parameter, i.e., phase difference $\Delta\phi$, is defined as $\Delta\phi = \phi_u - \phi_d$, where $\phi_u$ and $\phi_d$ are the operational phase angles of the

upstream actuator and of the downstream actuator, respectively. Its influence has been well studied in previous works [23, 24] and hence is only briefly summarized here. Generally three different types of flow structures are observed, i.e. one combined vortex, two completely separated vortices, and partially interacting vortex structures. Take case 4 as an example. At $\Delta\phi = \pi/2$ in Fig. 8b, the vortices produced from the two SJs perfectly merge together, forming a new vortex structure with a larger head and more strength. At $\Delta\phi = 3\pi/2$ in Fig. 8d, the resulting flow structures are a sequence of vortices with the same color appearing alternatively, seeming like doubling the frequency of the single SJ. At $\Delta\phi = 0$ and $\pi$, the two vortices produced by the twin SJ actuators are close, with the head of one vortex coupled with the legs of the other, forming complex vortex structures as shown in Figs. 8a and 8c. And in both the cases, the head of leading vortex is almost unaffected while that of trailing vortex is less sustainable, which was also observed in previous PIV measurements [28].

The three different types of vortex structures observed in the present dye visualization study can be used to explain previous hotwire results obtained in previous study. Liddle & Wood [26] measured the velocity field of in-line twin SJs in a turbulent boundary layer at various phase differences. The power spectral density analysis of the velocity history at a near-wall point in the mid-span plane showed that the spectral peak coincides with the operating frequency of the SJ actuator at most of the investigated phase differences. Although their crossflow and actuator operating conditions are different from those in the present study, at a specific phase difference that happens to

be $\Delta\phi = \pi/2$, the highest spectral peak is obtained, indicating the merge of vortex structures produced by the two actuators similar to in Fig. 8b. Furthermore, at another specific phase difference that happens to be $\Delta\phi = 3\pi/2$, the spectral peak occurs at twice the value of the actuator operating frequency, indicating the completely separated vortices produced by the two SJ actuators similar to in Fig. 8d.

### 3.3 A model for prediction of vortex patterns

Based on the observation of the resulting vortex structures, especially those generated at different phase differences, a formula can be proposed to predict the vortex patterns produced by in-line twin SJs. The spacing between the two vortices produced by in-line twin SJs is a function of the crossflow speed $U_\infty$, SJ actuator operating frequency $f$ , center-to-center distance between the two orifices $d$, and phase difference $\Delta\phi$. During one actuation cycle $T$, the head of a vortex structure travels a streamwise distance $\alpha U_\infty T = \alpha U_\infty / f$ , where $\alpha$ is a coefficient describing the ratio of the mean translating speed of the vortex structure over one actuation cycle to the crossflow speed. Since at the initial stage the vortex structure has to travel in the boundary layer, $\alpha$ is a value not greater than unity, i.e., $\alpha \leqslant 1$. By introducing the phase difference $\Delta\phi$, the non-dimensional spacing between the two SJ vortices, $s$, can be estimated as

$$s = \left(d - \frac{\alpha U_\infty}{f}\frac{\Delta\phi}{2\pi}\right)\Big/\frac{\alpha U_\infty}{f} = \frac{d}{D_o}\frac{St}{\alpha} - \frac{\Delta\phi}{2\pi} \tag{8}$$

Equation 8 indicates that s is a function of the non-dimensional orifice spacing $d/D_o$, Strouhal number $St$, vortex-crossflow speed ratio $\alpha$, and phase difference $\Delta\phi$. A value close to zero means the two vortices merge together, a positive value indicates the

vortex produced by the upstream actuator follows its counterpart produced by the downstream actuator, and a negative value indicates the opposite pattern. In addition, a value close to 0.5 or −0.5 indicates that the two vortices are completely separated. To use this formula, one has to determine the $\alpha$ value first. For the in-line twin SJ configuration, $\alpha$ can be affected by the operation of the downstream actuator. Since in the present study this influence is observed to be very weak, $\alpha$ is estimated from the single SJ visualization results. With this method, it is found that $\alpha$ varies with the Strouhal number St, e.g., $\alpha = 0.65$ at $St = 0.091$, and $\alpha = 0.75$ at $St = 0.045$.

The calculated $s$ values for all the investigated cases are listed in table 1, and the corresponding flow structures are shown in Fig. 9. For cases 1, 3-5 and 8-10 with $St = 0.091$, the normalized spacing at $\Delta\phi = \pi/2$ is $s = 0.03$ that is close to zero. The resulting flow structure is identified as one combined vortex. The normalized spacing at $\Delta\phi = 0$ is $s = 0.28$, meaning the vortex produced by the upstream actuator follows its counterpart produced by the downstream actuator, and they are partially interacted. The resulting flow structure is then a partially interacting vortex structure. At $\Delta\phi = \pi$ the normalized spacing is $s = -0.22$, meaning the vortex produced by the upstream actuator leads its counterpart. The resulting flow structure is also a partially interacting vortex structure. At $\Delta\phi = 3\pi/2$ the normalized spacing is $s = -0.47$ that is close to −0.5, and the resulting flow structure is identified as two completely separated vortices.

Things become different for cases with $St = 0.045$. It is found that the zero $s$ value falls between $\Delta\phi = 0$ and $\Delta\phi = \pi/2$, meaning the resulting vortex structure at these two phase differences slightly deviates from one combined vortex. This can be

confirmed by the visualization results of cases 2, 6 and 7 as shown in Fig. 9. At $\Delta\phi = \pi$ the normalized spacing is $s = -0.38$. The resulting vortex structure appears two completed separated vortices, because the larger vortex spacing involved at the present Strouhal number. At $\Delta\phi = 3\pi/2$, the normalized spacing is $s = -0.63$. As a result, instead of being close to its counterpart, the vortex produced by the upstream actuator is even closer to the vortex produced in the preceding actuation cycle.

**4. Conclusions**

A parametric study is conducted on the interaction of in-line twin circular SJs in different laminar crossflows and under different actuation conditions. For simplicity, the distance between the two SJ actuators is fixed at $d/D_o = 2$. Two-plane color dye visualization in a water tunnel is utilized. The four independent non-dimensional parameters that characterize the behavior of the twin SJs are identified, i.e., the Reynolds number $Re_L$, Strouhal number $St$, velocity ratio $VR$, and phase difference $\Delta\phi$. For the first time, the impact of these parameters on the interaction of twin SJs are examined. The increase of $Re_L$ not only results in the increase of circulation carried by SJ-induced vortices, but also induces instability, making the vortex structures more turbulent. As a result, the interaction between the twin SJs is less organized. With the increase of $VR$, the orientation angle between the emerging vortex structures and the plate increases, and the trajectories of the vortex heads are pushed away from the wall. As such, the interaction of the twin SJs occurs in a higher region, and the resulting vortex structures are more sustainable due to the escape of the near-wall high-shear region.The increase of St results in the decrease of the streamwise spacing between two

consecutive vortex structures. But it has no obvious influence on the twin SJ interaction. At different $\Delta\phi$ values, three types of vortex structures are identified: one combined vortex, two completely separated vortices, and a partially interacting vortex structure. Based on the flow patterns induced by twin SJs under various working conditions, a simple but useful formula is proposed to predict the resulting vortex pattern from the twin SJ interaction.

Although promising, it must be admitted that some issues have to be addressed before the proposed formula, equation 8, can be used with confidence. First, the term $\alpha$ is a parameter relating the convection velocity of SJ-induced vortex structures to the crossflow velocity. To determine its value, instead of using observation from the single SJ visualization, a quantitative analysis of the boundary layer properties and the vortex properties is necessary, which, however, is out of the scope of the present qualitative study. Second, the term $d/D_o$ that quantifies the spacing between the twin SJs is fixed in the present study. Since it influences the extent of interaction between the twin SJs and hence their spacing s, an investigation on its effect is also necessary. In the near future, therefore, studies will be conducted to address these two issues, so that the applicability of the present formula can be further validated.

## ACKNOWLEDGMENT

The first author of this paper, Dr. Xin Wen, would like to acknowledge the financial support from Nanyang Technological University for his Ph.D. study.

## REFERENCES

[1] Seifert, A., and Pack, L. G., 1999, “Oscillatory control of separation at high Reynolds numbers,” AIAA Journal, **37**(9), pp. 1062-1071. DOI: 10.2514/2.834

[2] Amitay, M., Smith, D. R., Kibens, V., Parekh, D. E., and Glezer, A., 2001, “Aerodynamic flow control over an unconventional airfoil using synthetic jet actuators,” AIAA Journal, **39**(3), pp.361-370. DOI: 10.2514/2.1323

[3] Amitay, M., and Glezer, A., 2002, “Role of actuation frequency in controlled flow reattach- ment over a stalled airfoil,” AIAA Journal, **40**(2), pp.209-216. DOI: 10.2514/2.1662

[4] Zhong, S., Jabbal, M., Tang, H., Garcillan, L., Guo, F., Wood, N., and Warsop, C., 2007, “Toward the design of synthetic-jet actuators for full-scale flight conditions,” Flow, Turbulence and Combustion, **78**(3), pp. 283-307. DOI: 10.1007/s10494-006-9061-3

[5] Yen, J. and Ahmed, N.A., 2012, “Parametric Study of Dynamic Stall Flow Field With Synthetic Jet Actuation,” ASME. Journal of Fluids Engineering, **134**(7), pp. 071106-8. DOI: 10.1115/1.4006957

[6] Tang, H., Salunkhe, P., Zheng, Y., Du, J., and Wu, Y., 2014, “On the use of synthetic jet actuator arrays for active flow separation control,” Experimental Thermal and Fluid Science, **57**, pp. 1-10. DOI: 10.1016/j.expthermflusci.2014.03.015

[7] Pavlova, A. A., Otani, K., and Amitay, M., 2008, “Active control of sprays using a single synthetic jet actuator,” International Journal of Heat and Fluid Flow, **29**(1), pp. 131-148. DOI: 10.1016/j.ijheatfluidflow.2007.06.004

[8] Al-Atabi, M., 2011, “Experimental Investigation of the Use of Synthetic Jets for Mixing in Vessels,” ASME. Journal of Fluids Engineering, **133**(9), pp. 094503-4. DOI: 10.1115/1.4004941

[9] Xia, Q., and Zhong, S., 2014, “Enhancement of laminar flow mixing using a pair of staggered lateral synthetic jets,” Sensors & Actuators A Physical, **207**, pp. 75-83. DOI: 10.1016/j.sna.2013.12.026

[10] Rathnasingham, R., and Breuer, K. S., 2003, “Active control of turbulent boundary layers,” Journal of Fluid Mechanics, **495**, pp. 209-233.DOI: 10.1017/S0022112003006177

[11] Crook, A., and Wood, N., 2001, “Measurements and visualisations of synthetic jets,” AIAA Paper, pp. 2001-0145.

[12] Ramasamy, M., Wilson, J. S., Martin, P. B., 2010, “Interaction of synthetic jet with boundary layer using microscopic particle image velocimetry,” Journal of Aircraft, **47**(2), pp. 404-422. DOI: 10.2514/1.45794

[13] Zhong S., and Zhang, S., 2013, "Further examination of the mechanism of round synthetic jets in delaying turbulent flow separation," Flow, Turbulence and Combustion, **91**(1), pp. 177-208. DOI: 10.1007/s10494-013-9469-5

[14] Jabbal, M., and Zhong, S., 2008, "The near wall effect of synthetic jets in a boundary layer," International Journal of Heat and Fluid Flow, **29**(1), 119–130. DOI: 10.1016/j.ijheatfluidflow.2007.07.011

[15] Zhou, J., and Zhong, S., 2010, "Coherent structures produced by the interaction between synthetic jets and a laminar boundary layer and their surface shear stress patterns," Computers & Fluids, **39**(8), pp. 1296-1313.DOI: 10.1016/j.compfluid.2010.04.001

[16] Wen, X., and Tang, H., 2014, "On hairpin vortex induced by circular synthetic jets in laminar and turbulent boundary layers," Computers & Fluids, 95, pp. 1-18. DOI: 10.1016/j.compfluid.2014.02.002

[17] Jabbal, M., and Zhong, S., 2010, "Particle image velocimetry measurements of the interaction of synthetic jets with a zero-pressure gradient laminar boundary layer," Physics of Fluids, **22**(6), pp. 063603. DOI: 10.1063/1.3432133

[18] Zhang, S., and Zhong, S., 2010, "Experimental investigation of flow separation control using an array of synthetic jets," AIAA Journal, **48**(3), pp. 611-623. DOI: 10.2514/1.43673

[19] Hasnain, Z., Trollinger, L.N., Hubbard, J.E., and Flatau, A.B., 2015, "Dynamic Flow Control over Aerodynamic Bodies using Phased Array Vectored Synthetic Jet Actuation," AIAA Paper, pp. 2015-2426.

[20] Zhao, G., Zhao, Q., Gu, Y., Chen, X., 2016, "Experimental investigations for parametric effects of dual synthetic jets on delaying stall of a thick airfoil," Chinese Journal of Aeronautics, **29**(2), pp. 346-557.DOI:10.1016/j.cja.2016.02.010.

[21] Kolar, V., Takao, H., Todorki, T., Savory, E., Okamoto, S., and Toy, N., 2003, "Vorticity transport within twin jets in cross flow," Experimental Thermal and Fluid Science, **27**(5), pp. 563-571. DOI: 10.1016/S0894-1777(02)00270-4

[22] Watson, M., Jaworski, A.J., and Wood, N.J., 2003, "Contribution to the understanding of flow interactions between multiple synthetic jets," AIAA Journal, **41**(4), pp. 747-749. DOI: 10.2514/2.2008

[23] Wen, X., and Tang, H., 2015, “Effect of phase difference on the interaction of hairpin vortices induced by in-line twin synthetic jets,” Journal of Visualization, **19**(1), pp. 79-87. DOI: 10.1007/s12650-015-0291-0

[24] Wen, X., Tang, H., and Duan, F., 2015, “Vortex dynamics of in-line twin synthetic jets in a laminar boundary layer,” Physics of Fluids, **27**, pp. 083601. DOI: 10.1063/1.4928216

[25] Wen, X., Tang, H., and Duan, F., 2016, “Interaction of in-line twin synthetic jets with a separated flow,” Physics of Fluids, **28**, pp. 043602. DOI: 10.1063/1.4946800

[26] Liddle, S. C., and Wood, N. J., 2005, “Investigation into clustering of synthetic jet actuators for flow separation control applications,” Aeronautical Journal, **109**(1091), pp. 35-44.

[27] Iai, T., Iwabuchi, K., Motosuke M., and Honami, S., 2010, “Vortex behavior of in-line synthetic jets in cross flow at low Reynolds number,” AIAA Paper, pp. 2010-4412.

[28] Honami, S., and Motosuke, M., 2012, “Vortex interaction of in-line synthetic jets injected at different phase in low Reynolds number cross flow,” AIAA Paper, pp. 2012-3243.

[29] Jabbal, M., Wu, J., and Zhong, S., 2006, “The performance of round synthetic jets in quies- cent flow,” Aeronautical Journal, **110**(1108), pp. 382-393. DOI: 10.1017/S0001924000001305

[30] Tang, H., and Zhong, S., 2006, “Incompressible flow model of synthetic jet actuators,” AIAA Journal, **44**(4), pp. 908-912. DOI: 10.2514/1.15633

[31] Zhou, J., Tang, H., and Zhong, S., 2009, “Vortex roll-up criterion for synthetic jets,” AIAA Journal, **47**(5), pp. 1252-1262. DOI: 10.2514/1.40602

[32] Holman, R., Utturkar, Y., Mittal, R., Smith, B. L., and Cattafesta, L., 2005, “Formation criterion for synthetic jets,” AIAA J., **43**(10), pp. 2110-2116. DOI: 10.2514/1.12033

[33] Milanovic, I. M., and Zaman, K. B. M. Q., 2005, “Synthetic jets in cross-flow,” AIAA Journal, **43**(5), pp. 929-940. DOI: 10.2514/1.4714

[34] Gharib, M., Rambod, E., and Shariff, K., 1998, “A universal time scale for vortex ring formation,” Journal of Fluid Mechanics, **360**, pp.121-140. DOI: 10.1017/S0022112097008410

Fig. 1

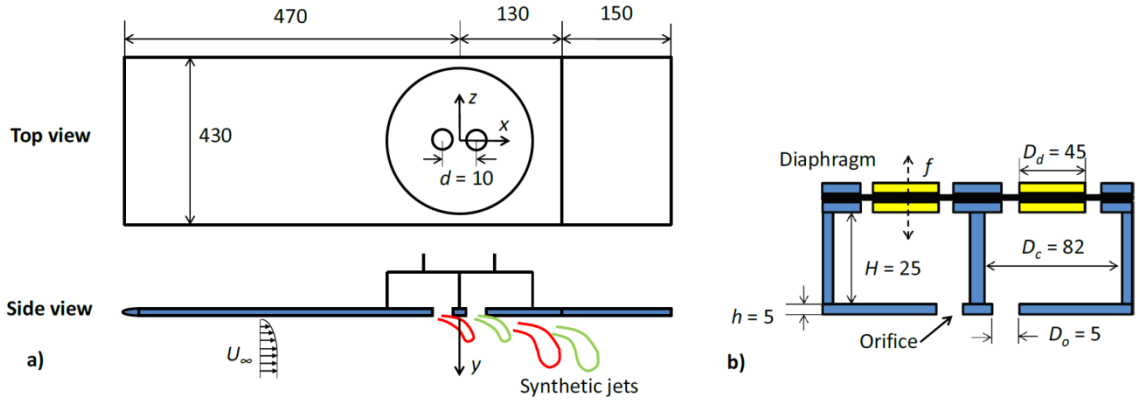


Schematic of (a) the test plate and (b) the twin SJ actuators (all numbers are in mm)

Fig. 2

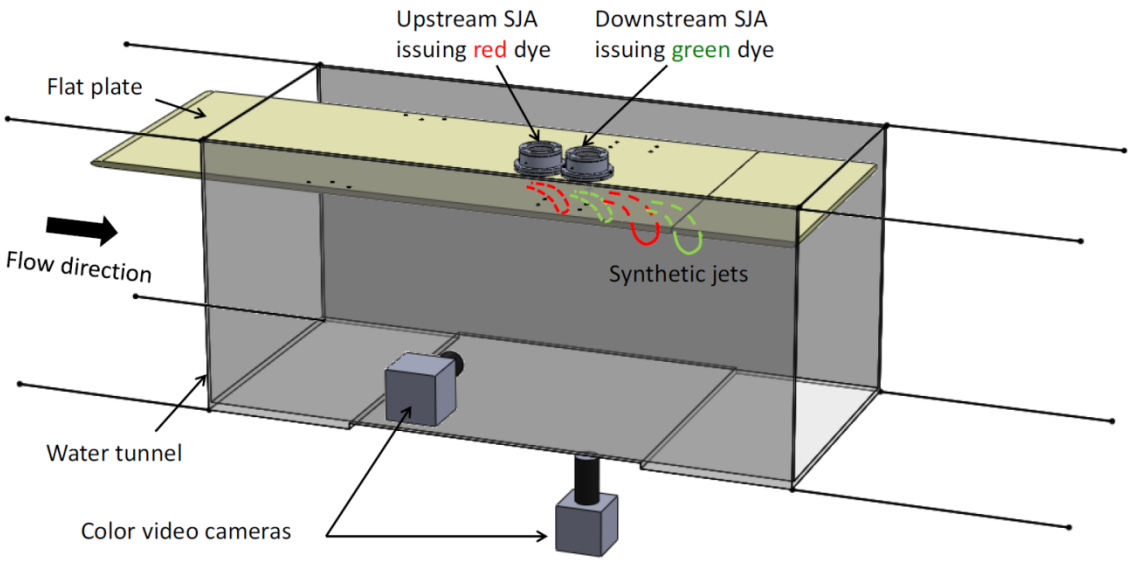


Schematic of the two-plane dye visualization system

Fig. 3

| Case | $U_\infty$ (m/s) | $\Delta$ (mm) | $f$ (Hz) | $L$ | $S$ | $Re_L$ | $St$ | $VR$ |
|---|---|---|---|---|---|---|---|---|
| 1 | 0.028 | 0.148 | 0.5 | 2.4 | 8.9 | 72 | 0.091 | 0.22 |
| 2 | 0.055 | 0.148 | 0.5 | 2.4 | 8.9 | 72 | 0.045 | 0.11 |
| 3 | 0.055 | 0.105 | 1 | 1.7 | 12.5 | 72 | 0.091 | 0.16 |
| 4 | 0.055 | 0.158 | 1 | 2.6 | 12.5 | 164 | 0.091 | 0.23 |
| 5 | 0.055 | 0.210 | 1 | 3.4 | 12.5 | 289 | 0.091 | 0.31 |
| 6 | 0.110 | 0.158 | 1 | 2.6 | 12.5 | 164 | 0.045 | 0.12 |
| 7 | 0.110 | 0.210 | 1 | 3.4 | 12.5 | 289 | 0.045 | 0.16 |
| 8 | 0.110 | 0.074 | 2 | 1.2 | 17.7 | 72 | 0.091 | 0.11 |
| 9 | 0.110 | 0.105 | 2 | 1.7 | 17.7 | 145 | 0.091 | 0.16 |
| 10 | 0.110 | 0.158 | 2 | 2.6 | 17.7 | 328 | 0.091 | 0.23 |

Case summary

Fig. 4

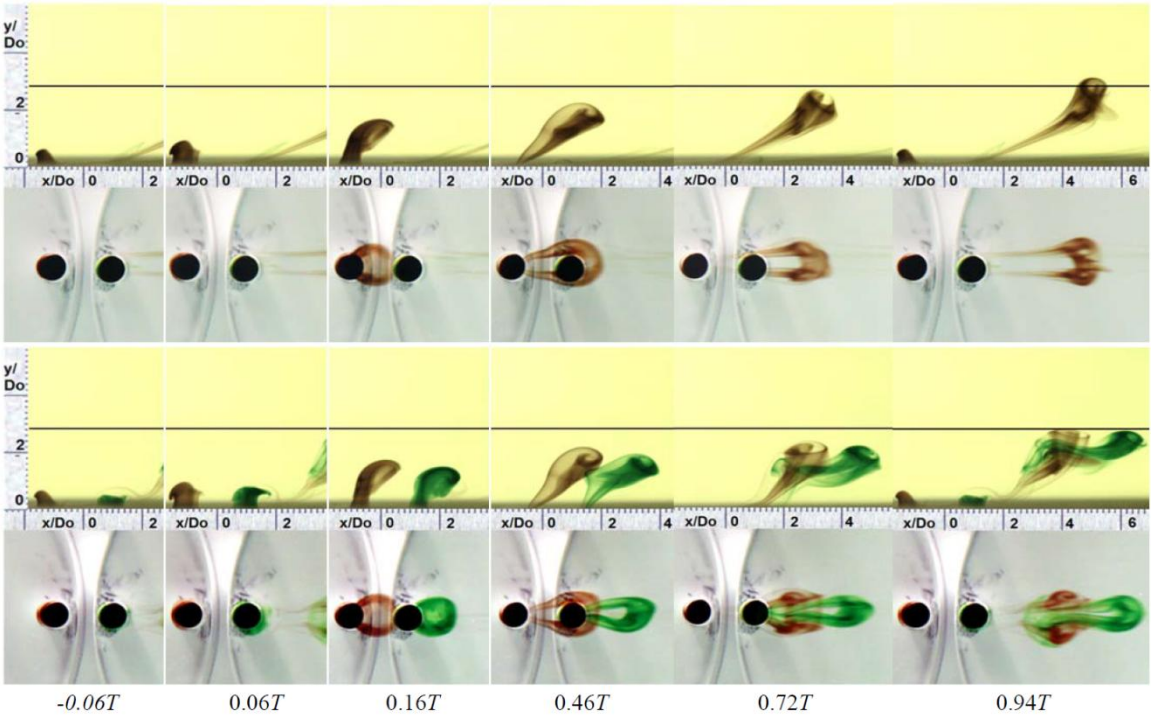


Evolution of vortex structures in a crossflow for case 4. Upper two rows: two-plane views of a single SJ. Bottom two rows: two-plane views of twin SJs with zero phase difference. The horizontal line represents the edge of the boundary layer.

Fig. 5

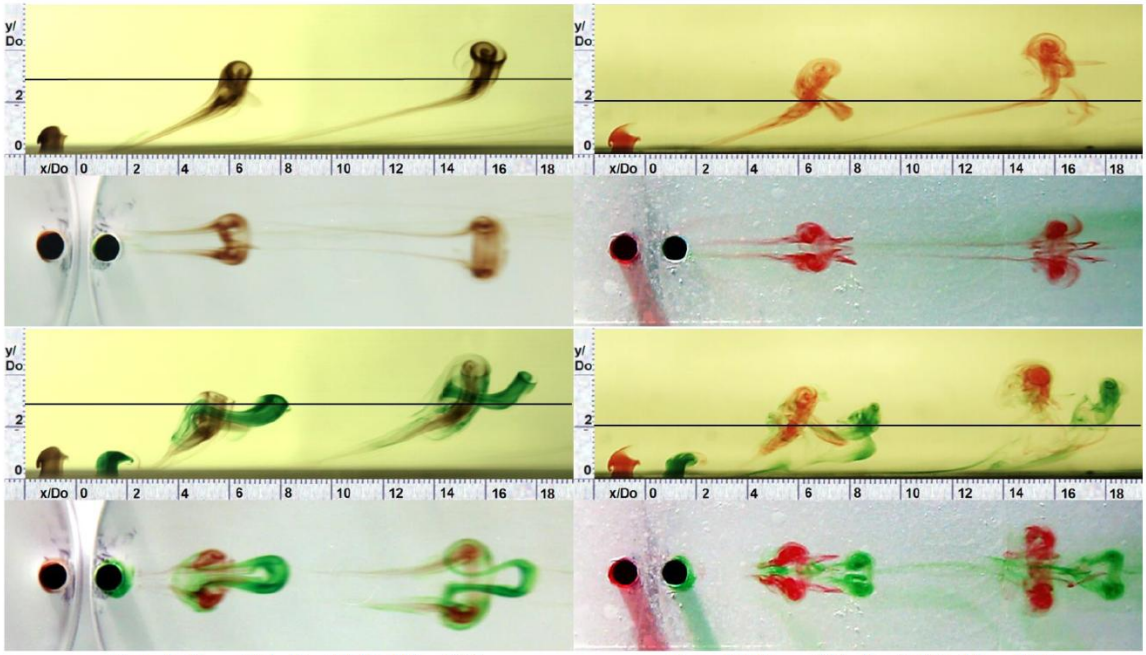


Case 4: $Re_L = 164$, $St = 0.091$, $VR = 0.23$ Case 10: $Re_L = 328$, $St = 0.091$, $VR = 0.23$

Two-plane dye visualization showing the influence of $Re_L$ on single- and twin-SJ induced vortex structures. The twin SJs are introduced with zero phase difference. The horizontal line represents the edge of the boundary layer.

Fig. 6

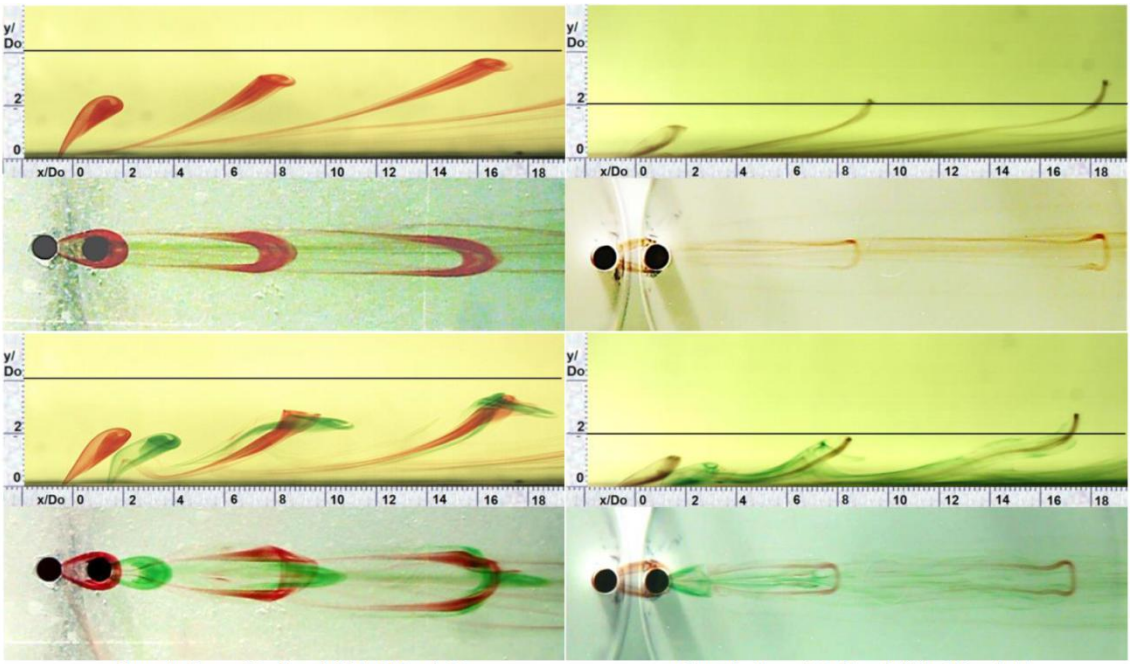


Case 1: $Re_L = 72$, $St = 0.091$, $VR = 0.22$ Case 8: $Re_L = 72$, $St = 0.091$, $VR = 0.11$

Two-plane dye visualization showing the influence of *VR* on single- and twin-SJ induced vortex structures. The twin SJs are introduced with zero phase difference. The horizontal line represents the edge of the boundary layer.

Fig. 7

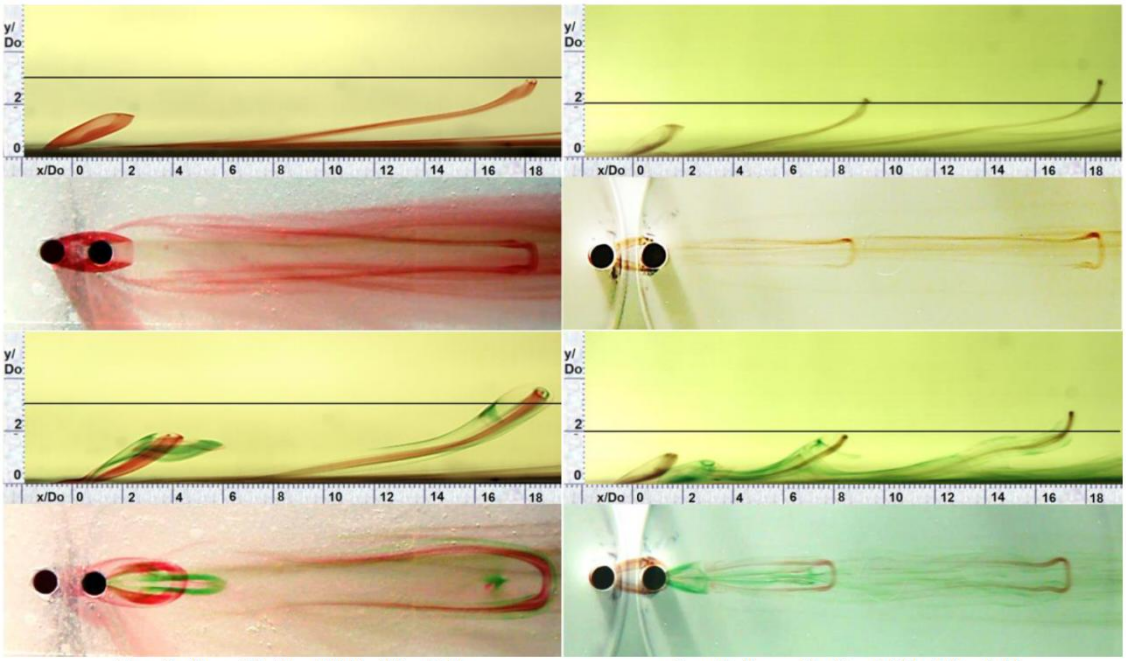


Case 2: $Re_L = 72$, $St = 0.045$, $VR = 0.11$ Case 8: $Re_L = 72$, $St = 0.091$, $VR = 0.11$

Two-plane dye visualization showing the influence of *St* on single- and twin-SJ induced vortex structures. The twin SJs are introduced with zero phase difference. The horizontal line represents the edge of the boundary layer.

Fig. 8

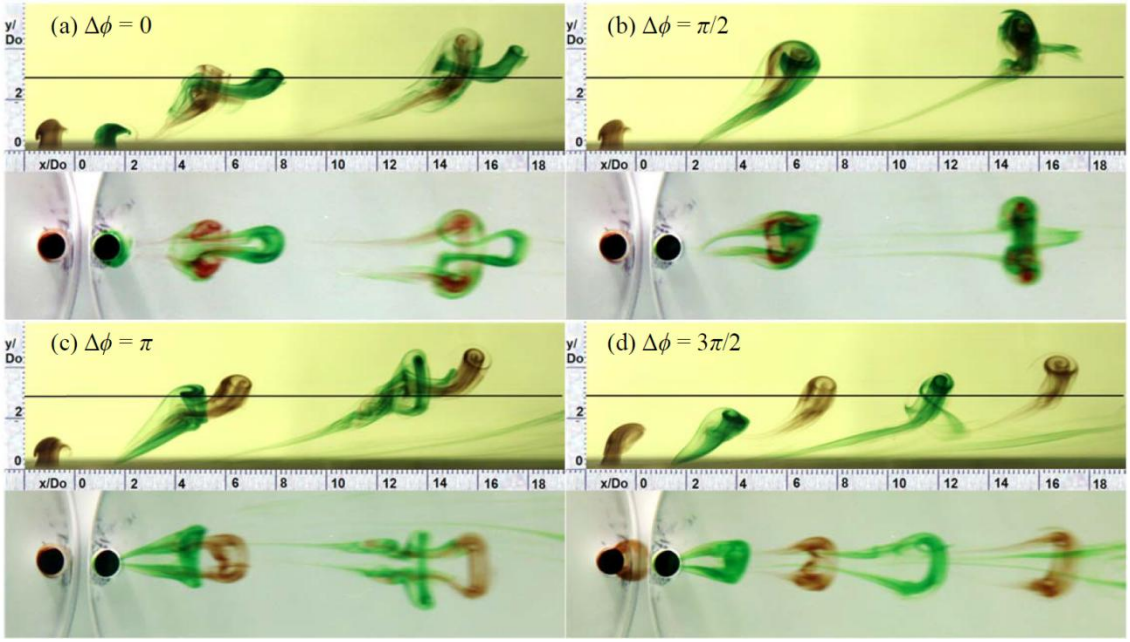


Two-plane dye images of the twin SJs at various phase differences for case 4. The horizontal line represents the edge of the boundary layer.

Fig. 9

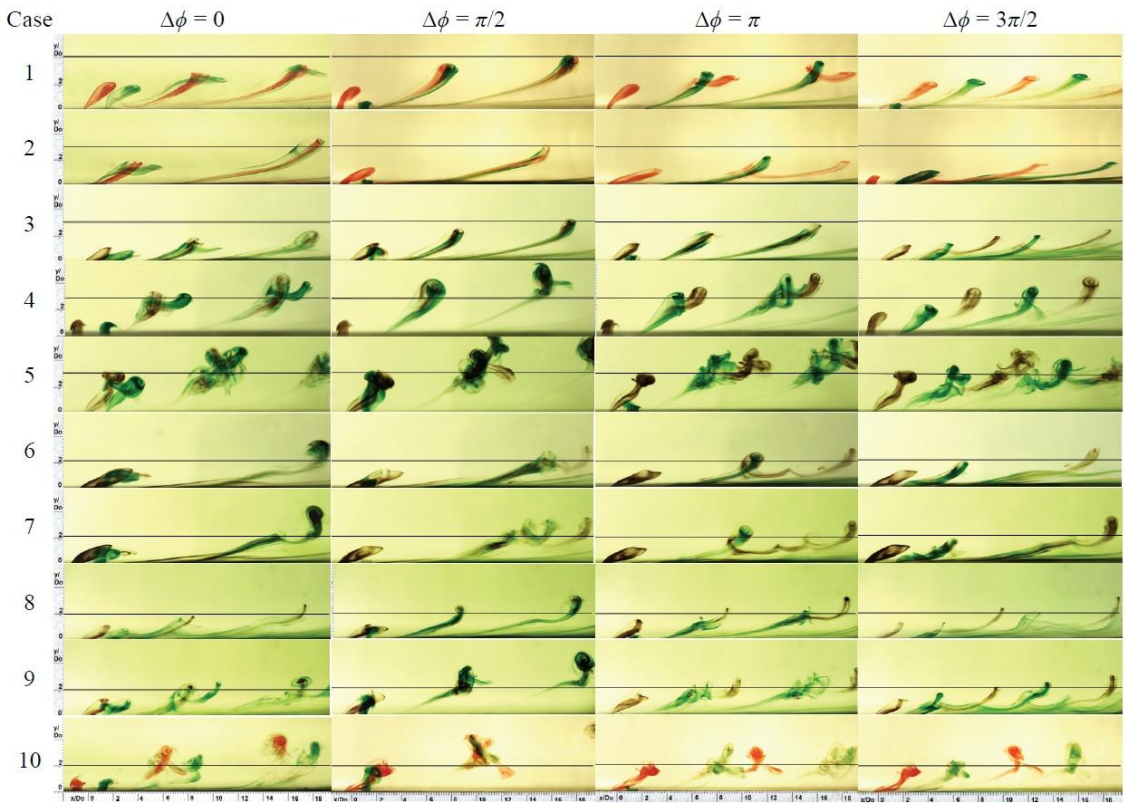


Summary of side view dye visualization at different phase difference for all cases, showing the spacing and resulting interaction between the vortices produced by the twin SJ actuators. The horizontal line represents the edge of the boundary layer.

Table 1

Estimation of $s$ value at different $St$ and $\Delta\phi$

| **Case** | $d/D_o$ | $St$ | $\alpha$ | $s$ ($\Delta\phi = 0$) | $s$ ($\Delta\phi = \pi/2$) | $s$ ($\Delta\phi = \pi$) | $s$ ($\Delta\phi = 3\pi/2$) |
|---|---|---|---|---|---|---|---|
| **1, 3-5, 8-10** | 2 | 0.091 | 0.65 | 0.28 | 0.03 | −0.22 | −0.47 |
| **2, 6, 7** | 2 | 0.045 | 0.75 | 0.12 | −0.13 | −0.38 | −0.63 |

**Figure Captions List**

Fig. 1 Schematic of (a) the test plate and (b) the twin SJ actuators (all numbers are in mm)

Fig. 2 Schematic of the two-plane dye visualization system

Fig. 3 Case summary

Fig. 4 Evolution of vortex structures in a crossflow for case 4. Upper two rows: two-plane views of a single SJ. Bottom two rows: two-plane views of twin SJs with zero phase difference. The horizontal line represents the edge of the boundary layer.

Fig. 5 Two-plane dye visualization showing the influence of $Re_L$ on single- and twin-SJ induced vortex structures. The twin SJs are introduced with zero phase difference. The horizontal line represents the edge of the boundary layer.

Fig. 6 Two-plane dye visualization showing the influence of *VR* on single- and twin-SJ induced vortex structures. The twin SJs are introduced with zero phase difference. The horizontal line represents the edge of the boundary layer.

Fig. 7 Two-plane dye visualization showing the influence of *St* on single- and twin-SJ induced vortex structures. The twin SJs are introduced with zero phase difference. The horizontal line represents the edge of the boundary layer.

Fig. 8 Two-plane dye images of the twin SJs at various phase differences for case 4. The horizontal line represents the edge of the boundary layer.

Fig. 9 Summary of side view dye visualization at different phase difference for all cases, showing the spacing and resulting interaction between the vortices produced by the twin SJ actuators. The horizontal line represents the edge of the boundary layer.

## Table Caption List

Table 1 Estimation of $s$ value at different $St$ and $\Delta\phi$